Title
Consolidation of cellular memory representations in superficial neocortex

Journal
iScience, 26(2)

ISSN
2589-0042

Authors
Esteves, Ingrid M
Chang, HaoRan
Neumann, Adam R
et al.

Publication Date
2023-02-01

DOI
10.1016/j.isci.2023.105970

Peer reviewed

iScience

CellPress
OPEN ACCESS

Article

Consolidation of cellular memory representations in superficial neocortex

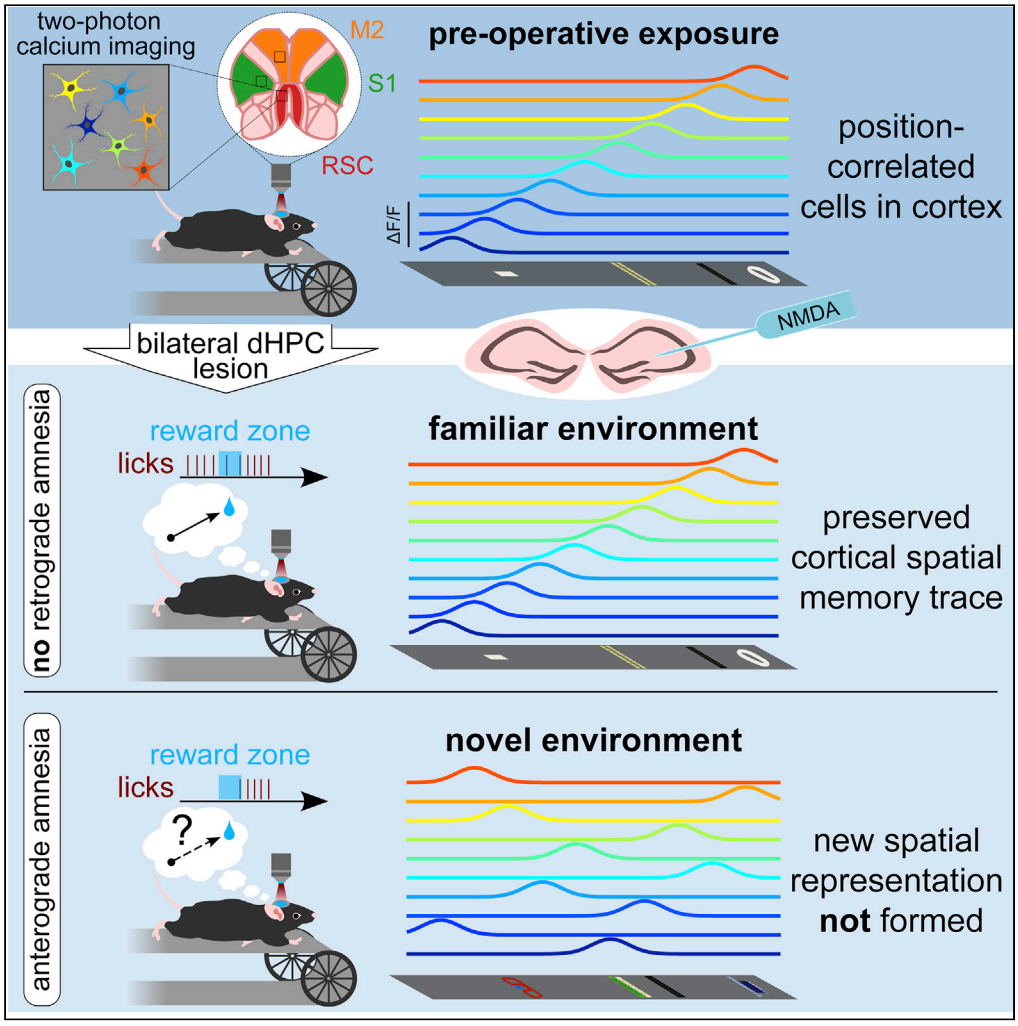

Ingrid M. Esteves, HaoRan Chang, Adam R. Neumann, Bruce L. McNaughton

ingrid.esteves@uleth.ca

Highlights

Two-photon imaging of position-correlated cortical cells in VR spatial navigation

Place encoding is rescued for familiar but not novel environment following HPC lesion

Preemptive licking at reward site demonstrates anterograde but not retrograde amnesia

Functional demonstration of the consolidation of hippocampal-dependent memory traces

Esteves et al., iScience 26, 105970
February 17, 2023
https://doi.org/10.1016/j.isci.2023.105970

iScience

CellPress
OPEN ACCESS

Article

Consolidation of cellular memory representations in superficial neocortex

Ingrid M. Esteves,[1,3,*] HaoRan Chang,[1] Adam R. Neumann,[1] and Bruce L. McNaughton[1,2]

SUMMARY

Systems-level memory consolidation, a key concept in memory research, involves the conversion of memories that depend on the hippocampus for their formation into efficient hippocampus-independent forms, presumably encoded by cortico-cortical connections. Yet, little is understood about the nature of consolidated neural codes at the cellular ensemble level. Mice require an intact hippocampus for "virtual" spatial learning and to develop neocortical representations of the corresponding experiences. We find that, whereas a novel virtual environment is neither learned nor represented in superficial cortex following severe damage to hippocampus, pre-operatively learned memories and their corresponding sparse and widespread neural ensemble representations in cortical layers II–III are preserved, a *sine qua non* of memory consolidation. These findings provide a new window for future study of the cellular mechanisms of memory consolidation.

INTRODUCTION

Damage to the hippocampal formation severely impairs acquisition of new, "episodic" memory.[1,2] This phenomenon may be related to the position of the hippocampus at the top of the hierarchy of neocortical association areas, and to the fact that the number of cortical neurons far exceeds the number of connections that can be supported by a given neuron (Schwindel & McNaughton, 2011, for review).[3] This connection sparsity means that formation of arbitrary associations in real time (especially long-range ones) would be difficult, because the necessary synapses between any two arbitrary active neocortical cells most likely do not exist *a priori*. The neocortex might overcome this problem through the rapid formation of *indirect* associations among its currently active neurons, mediated by a common, top-down pattern from the hippocampus. According to this view, each unique experience generates a corresponding unique, sparse pattern in hippocampus, which serves as a context or "index"[4–6] to the set of currently active cortical neurons. These patterns are unique to the location and the nature of each experience (e.g. Leutgeb et al.[7]). Associative plasticity in the feedback projections from the hippocampus (the "index") to the corresponding active cortical cells (the "attributes") would enable subsequent retrieval of the memory attributes. Thus, at least initially, the memory becomes encoded as connections between hippocampus and cortex, rather than among cortical cells directly. Some memories and learned behaviors never lose their dependence on an intact hippocampus; however, some become resistant over time to hippocampal damage,[8] suggesting that appropriate cortico-cortical connections, sufficient to substitute for the hippocampo-cortical ones, develop over time and become dominant. This process may also accompany the extraction of structure from the memory into the cortex's "semantic" knowledge,[9–15] which generally survives hippocampal loss. While there has been much study of the behavioral and gene-expression dynamics of this memory consolidation process, there has been little investigation at the cellular encoding level into the nature and location of such hippocampus-independent memory representations in the cortex.

Recent studies have shown that, during traversals of a sequence of locations (either real or virtual), cortical neurons, especially in superficial cortex, develop sparse, position-correlated sequences of neural activity,[16–19] much as in the hippocampus. In intact mice, position-correlated cells emerge in cortex within a few sessions in a novel virtual "environment", consisting of a treadmill belt with attached "spatial" cues,[20] but develop poorly in mice with dorsal hippocampal lesions.[16,17] Here, we show that superficial cortical representations of a pre-operatively learned virtual environment are retained following hippocampal lesions, as is the corresponding spatial memory, whereas the same mice neither learn a post-operatively novel environment nor represent it as position-correlated cells in superficial cortex.

[1]Canadian Centre for Behavioural Neuroscience, Department of Neuroscience, University of Lethbridge, 4401 University Drive, Lethbridge, AB T1K 3M4, Canada

[2]Department of Neurobiology and Behaviour, University of California, Irvine, Irvine, CA 92697, USA

[3]Lead contact

*Correspondence: ingrid.esteves@uleth.ca

https://doi.org/10.1016/j.isci.2023.105970

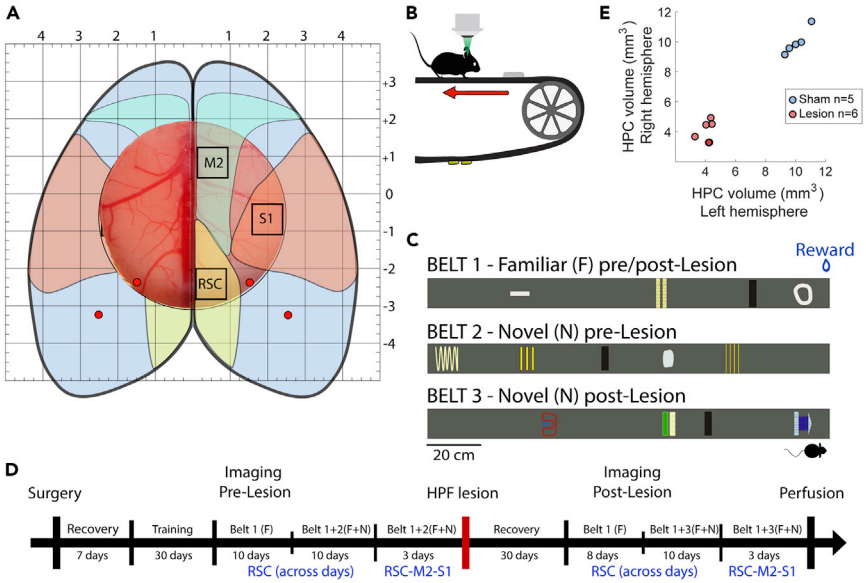

Figure 1. Two-photon calcium imaging of cortical neuronal ensembles before and after hippocampal lesion

(A) A cranial window was implanted over dorsal neocortex and 3 ROIs were imaged: secondary motor cortex (M2), primary somatosensory cortex (S1), and the retrosplenial cortex (RSC).

(B) Mice repeatedly traversed 150-cm long linear treadmill belts lined with tactile cues to receive reward at a specific location.

(C) Schematics of the three belts (illustrated to scale on the x axis).

(D) Experimental timeline. Following implantation of the imaging window, animals were trained to run head-fixed on a treadmill. Subsequently, mice were exposed to the "familiar" belt, while imaging was carried out in RSC. The pre-lesion novel belt was then introduced and tested with the familiar belt alternating within session. On the last 5 pre-surgery days, all three cortical regions were imaged. Lesion of the dorsal hippocampi (or sham) was then carried out, followed by a one-month recovery period. During the post-operatively phase, the same imaging protocol was carried out, in which the first novel belt was substituted for a different one, which the animals were never exposed to before the lesion/sham surgery, while also running on the pre-operatively familiar belt.

(E) Scatterplot of the hippocampus (HPC) volume for both hemisphere for the sham and lesion group.

RESULTS

Two-photon Ca^{2+} imaging was used to record neural activity in mice during head-fixed running on treadmill belts containing several visuo-tactile cues (Figure 1; STAR Methods), before and after bilateral lesions of dorsal hippocampus. Animals were tested on the same "familiar" belt before and after hippocampal lesions (or sham surgeries). "Novel" belts with different cue sets were employed for the pre- and post-operative (lesion/sham) periods following (re)acquaintance with the "familiar" belt. We tracked neuronal activity in three neocortical areas: retrosplenial cortex (RSC), secondary motor cortex, and primary somatosensory cortex.

Hippocampal lesion causes anterograde but not retrograde amnesia for reward locations in virtual spatial environments

Each belt had a particular virtual location where water reward was delivered (Figure 1C). Pre-operatively, both groups expressed similar behavior in both familiar and novel environments Figure S2. The post-operative running speeds in the familiar and novel belts were also similar between sham and lesion groups. Post-operatively, sham and lesion groups made a comparable number of attempts at licking the reward port throughout the experiment (Figure 2-left); however, the distributions of licks in the novel environment were significantly different between groups. For the sham group, an overwhelming proportion of licks were concentrated at the reward site in both familiar and novel environments. The same behavior was exhibited by the lesion group in the familiar environment; however, in the novel environment, the lesioned mice licked mostly outside of the reward zone. (Figure 2-middle, right). Thus, pre-operative memory was retained, but learning in the novel environment was seriously impaired. This is the defining feature of the memory consolidation concept.

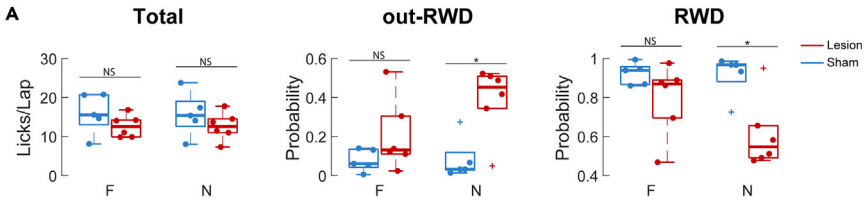

Figure 2. Hippocampal lesion produced behavioral deficits in learning the reward site in a novel environment, while memory for the reward location in the pre-operatively learned environment was preserved

(A) Boxplot of the total number of attempts at licking the reward spout per lap for the sham (blue) and the lesion group (red), in both familiar and novel environments post-operatively (left). Boxplot of the licking probability outside the reward zone (out-RWD; middle), and inside the reward zone (RWD; right) during the last sessions. Reward site is the 3 cm preceding and following the reward. Dots: Average over the last three sessions for each animal. Line: median; box: 25th and 75th percentiles; whiskers: minimum and maximum values; + signs: outliers; NS not significant, and *p < 0.05 [Independent-Samples Kruskal-Wallis Test].

Cortical neurons preserve encoding of a familiar spatial environment following hippocampal lesion, but encoding of a novel environment fails to form

We used relatively liberal criteria (see STAR Methods) to categorize cells as "spatially selective" and to define cells' "place fields". Overall, there were no between-group (lesion vs sham) or between-environment (F, N) differences in any of the three cortical regions in the proportion of cells that passed the selectivity threshold, which was overall about 40% with these liberal criteria (Figure S3A). However, for the novel environment, cells meeting the selectivity criteria were overall much less spatially selective and collectively formed a less uniform population encoding of the belt in the lesion group (Figures 3A and 3B). This difference was associated with an increase in the proportions of lesion-group cells with multiple place fields, instead of a single one (Figure S3B).

The emergence of layer II–III cortical position encoding was quantified using measures of spatial information content on a per neuron basis[21] for all cells passing the spatial selectivity threshold. Some forgetting was expected in the 30 days break between the last pre-lesion/sham session and the first post-operatively sessions. Indeed, there was a time-dependent degradation (forgetting) of spatial information content in the familiar environment; however, the familiar memory recovered over sessions in both lesion and sham mice, with no between-group difference (Figure 3C-top). The sham mice showed normal acquisition of the cortical representation of the novel environment (Belt 3); however, the lesion group showed very little spatial information in the novel environment in RSC (Figure 3C-bottom). In all cortical regions, neurons' spatial information content was similar between sham and lesion for the familiar environment, while this quantity was significantly reduced in the lesion group for the novel environment (Figures 3D and 3E).

We quantified the reliability of spatial coding at the population level by computing the error of lap-by-lap position decoding, using a Bayesian decoder (STAR Methods). During the post-operative phase, the distribution of decoded position as a function of the animal's location indicates that the decoder from the lesion group in the novel environment gives a less accurate estimation of position (Figure 4A). There was a substantial increase (~2 x) in decoding error in the novel environment in all three cortical regions, in the lesion group, but not in the sham group, and none in the familiar environment in any group (Figure 4B).

DISCUSSION

Overall, whereas hippocampal lesions severely impaired the emergence of position-correlated cells representing a novel virtual environment, and similarly impaired spatial learning in that novel context, the representation of a pre-operatively exposed familiar environment and the memory for the reward location in that environment were spared. Lesioned mice's spatially selective firing activity in the novel environment was biased toward firing in the vicinity of the salient cues. Non-selective or weakly selective responses at the salient cues were common in the lesioned mice in the novel environments, giving rise to multiple "place" fields, which may have contributed to the higher spatial decoding error. The lesions themselves damaged 50% or more of the dorsal hippocampus, but left the ventral hippocampus largely intact (Figure 1E). Therefore, we cannot conclude that the preserved memory was entirely independent of

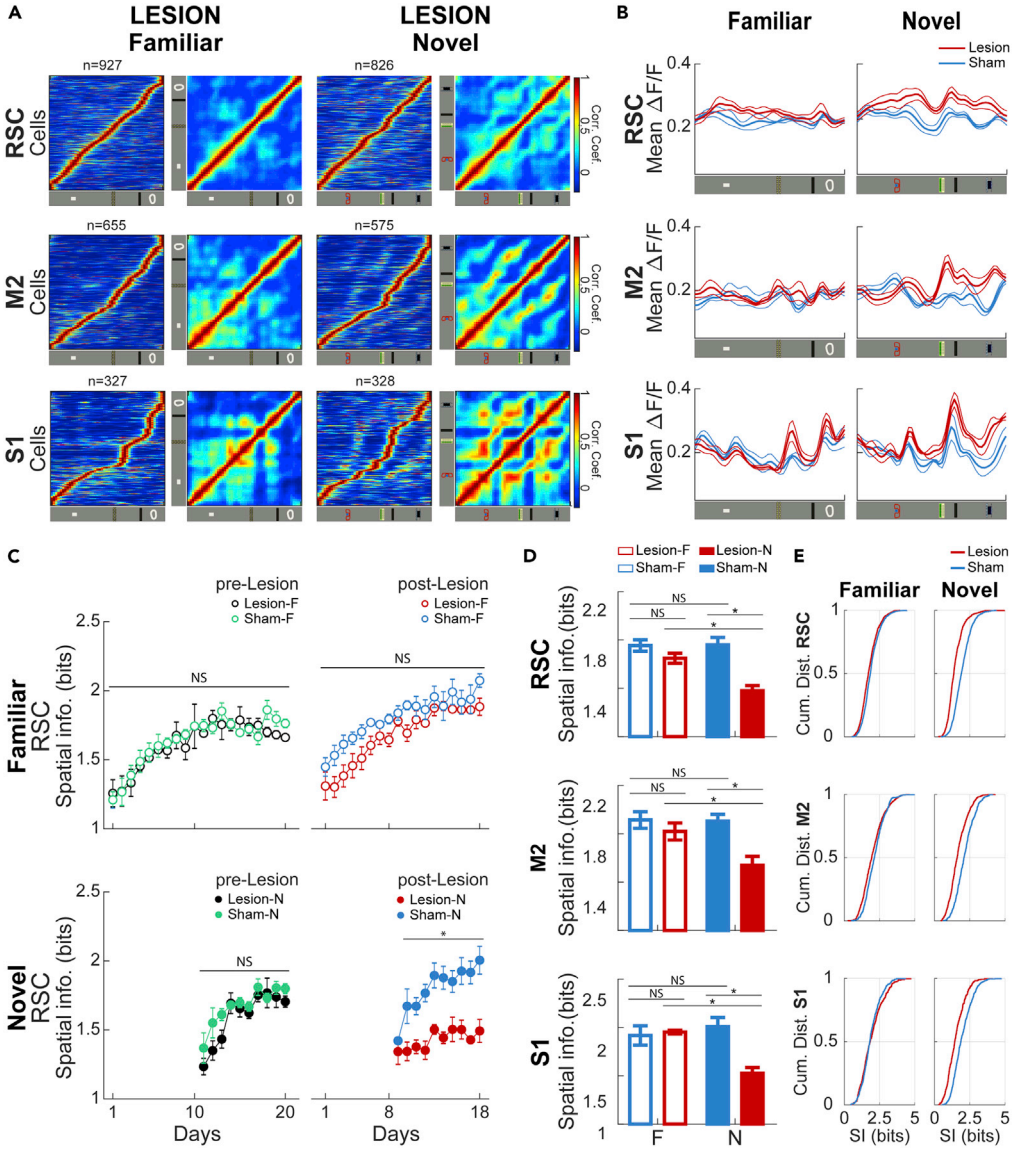

Figure 3. Hippocampal lesion impaired cortical representation of VR position for a newly experienced environment, while the encoding of an environment learned before lesion was spared

(A) Average response-tuning curves (min-max normalized) of spatially receptive cells as a function of location in the novel and familiar environments pooled across all lesion animals and segregated by cortical region. Accompanying are the Pearson correlation matrices of population vectors (columns of the response matrices) correlated over space.

(B) Average spatial-tuning curves of all cells passing the spatial selectivity threshold as a function of location in the novel and familiar environments, pooled across all lesion animals and segregated by cortical region (tuning curve normalized for each cell by: $\hat{r}(x) = \frac{r(x) - r_{min}}{r_{max}}$, where $\hat{r}(x)$ and $r(x)$ is the is the normalized and non-normalized tuning curves for each cell, r_{min} and r_{max} is the minimum and maximum values for each tuning curves, respectively).

(C) Average spatial information content (SI) of spatially selective cells in the RSC over consecutive days of exposure to the novel and familiar environments.

(D) Average spatial information conveyed by spatially selective neurons post-lesion for the novel and familiar environments in sham and lesion groups, segregated by cortical region during the last sessions, after spatial information of the two environments stabilized.

(E) Empirical cumulative distribution functions of the post-operatively spatial information for the sham (blue) and lesion groups (red) in the familiar (left) and novel (right), during the last sessions segregated by cortical regions. Error bars denote SEM over animals. NS not significant, *$p < 0.05$, **$p < 0.01$, and ***$p < 0.001$ [two-way repeated-measures ANOVA with Bonferroni adjustment for multiple comparisons in (C) and (D)].

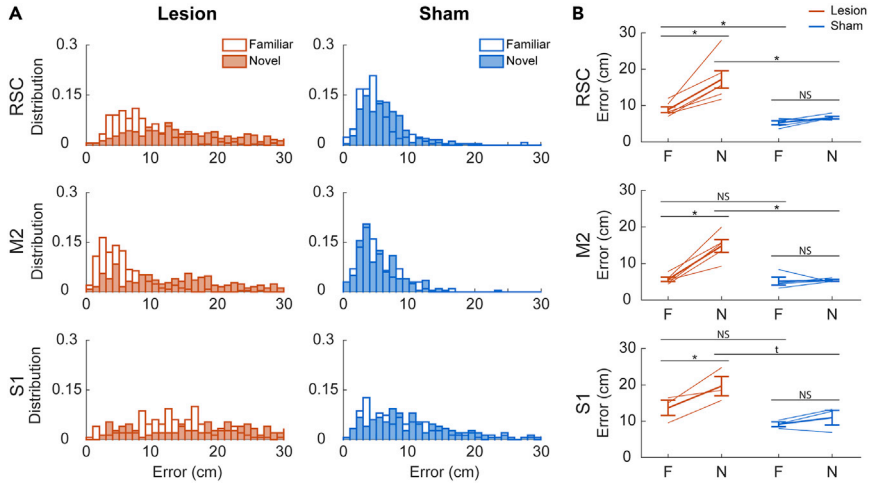

Figure 4. Following lesion of the hippocampus animal location in a novel environment could not be accurately decoded from the population activity

(A) Distribution functions of the absolute post-operatively decoding error for the sham (blue) and lesion groups (red) in the familiar (white) and novel (solid) bars.

(B) Mean decoding error for the sham and lesion groups in the novel and familiar environments post-operatively, segregated by cortical region (error bars denote SEM over animals). In all cortical regions, the average decoding error was increased for the lesion group from familiar to novel environments, while the error was comparable in the sham group. NS not significant, *$p < 0.05$, **$p < 0.01$, ***$p < 0.001$, and $^{t}p = 0.061$ [two-way repeated-measures ANOVA with Bonferroni adjustment for multiple comparisons].

hippocampal outflow[22] although many studies show that it is the dorsal hippocampus that is predominantly necessary for spatial learning[23,24] and whose output is focused on the retrosplenial cortex.[25–28] Both groups exhibited a decline in the spatial tuning for the familiar environment during the ~30 days interval between the last pre-lesion/sham trial and the first post-lesion/sham trial. Whether this was due to the mere passage of time or the surgical procedure (e.g., anesthesia) is unknown; however, these dynamics indicate that some trace of the previous coding was preserved, whereas new encoding was impaired. One possible explanation for the decline in the spatial tuning over the 30-day period is that the intact hippocampus enables the formation of new synaptic connections in cortex which may lose efficacy over time but physically persist, so that they can be re-potentiated upon re-exposure to the familiar environment. Another explanation is that the coding is preserved in deeper layers of the cortex, which were not accessible to imaging in these studies. It is well known that the re-exposure to a familiar environment is not essential for memory consolidation processes to occur; they can also happen during "offline" period like slow-wave sleep.[4] However, the retrieval of consolidated processes may require re-exposure in the absence of the hippocampus.

Overall, the present results show that an intact hippocampus enables superficial cortex to develop sparse, selective representations of the experience of being at particular locations under a particular behavioral and sensory context, and that these emergent neural codes persist after hippocampal damage sufficient to prevent new learning at the neural and behavioral levels under similar conditions. These findings provide a new framework in which to study the cellular and molecular foundations of long-term, hippocampus-independent memory.

Limitations of the study

Given the limited sample size, only a single cortical area out of three regions of interest could be assessed with reasonable statistical power during the exposure/re-exposure phases of the experiments, over successive recording days. We chose the retrosplenial cortex in consideration for the fact that it receives direct projections from the dorsal hippocampus.[25–28] We observed that following hippocampal lesion, neuronal representation of a familiar environment in the retrosplenial cortex is gradually reacquired with repeated re-exposures. However, this does not rule out the fact that other cortical areas may recover at a faster rate. Furthermore, it is possible that exchanges between distributed regions may contribute to this recovery,

which cannot be determined unless two or more regions are simultaneously evaluated. How spatial memory traces are preserved and "re-potentiated" across different cortical areas, following hippocampal loss, therefore remain to be determined.

STAR★METHODS

Detailed methods are provided in the online version of this paper and include the following:

- KEY RESOURCES TABLE
- RESOURCE AVAILABILITY
  - Lead contact
  - Materials availability
  - Data and code availability
- EXPERIMENTAL MODEL AND SUBJECT DETAILS
  - Ethics
- METHOD DETAILS
  - Experimental design
  - Head plate and imaging window implantation
  - Treadmill training and two-photon imaging
  - Hippocampal lesion
  - Image pre-processing
  - Place field analysis
  - Bayesian decoder
  - Histology
- QUANTIFICATION AND STATISTICAL ANALYSIS

SUPPLEMENTAL INFORMATION

Supplemental information can be found online at https://doi.org/10.1016/j.isci.2023.105970

ACKNOWLEDGMENTS

We thank Dr. M. Mohajerani for supervision/administration of microscope and animal breeding facilities, Jennifer Tarnowsky for logistics support, and Valerie Lapointe and Karim Ali for technical support, and WestGrid and Compute Canada for IT support. B.L.M. acknowledges funding from NIH Research Project Grant Program (R01) [no. NS121764], Defense Advanced Research Projects Agency (DARPA) [no. HR0011-18-2-0021], Natural Sciences and Engineering Research Council of Canada (NSERC) [no. 1631465], and Canadian Institutes of Health Research (CIHR) [no. PJT 156040]. H.C. is supported by the Canada Graduate Scholarships for Doctoral Program (NSERC CGS-D).

AUTHOR CONTRIBUTIONS

I.M.E. and B.L.M. conceptualized the experiment. I.M.E. and A.R.N. conducted the experiments and collected the data. I.M.E., H.C., and B.L.M. analyzed and interpreted the data. I.M.E., H.C., and B.L.M. wrote the manuscript, which all authors helped to revised.

DECLARATION OF INTERESTS

Authors declare that they have no competing interests.

INCLUSION AND DIVERSITY

We support inclusive, diverse, and equitable conduct of research.

Received: October 7, 2022
Revised: November 18, 2022
Accepted: January 10, 2023
Published: February 17, 2023

REFERENCES

1. Scoville, W.B., and Milner, B. (1957). Loss of recent memory after bilateral hippocampal lesions. J. Neurol. Neurosurg. Psychiatry *20*, 11–21. https://doi.org/10.1136/jnnp.20.1.11.

2. Yonelinas, A.P., Kroll, N.E.A., Quamme, J.R., Lazzara, M.M., Sauvé, M.J., Widaman, K.F., and Knight, R.T. (2002). Effects of extensive temporal lobe damage or mild hypoxia on recollection and familiarity. Nat. Neurosci. *5*, 1236–1241. https://doi.org/10.1038/nn961.

3. Schwindel, C.D., and McNaughton, B.L. (2011). Hippocampal-cortical interactions and the dynamics of memory trace reactivation. Prog. Brain Res. *193*, 163–177. https://doi.org/10.1016/B978-0-444-53839-0.00011-9.

4. McNaughton, B.L. (2010). Cortical hierarchies, sleep, and the extraction of knowledge from memory. Artif. Intell. *174*, 205–214. https://doi.org/10.1016/j.artint.2009.11.013.

5. Teyler, T.J., and DiScenna, P. (1986). The hippocampal memory indexing theory. Behav. Neurosci. *100*, 147–154. https://doi.org/10.1037/0735-7044.100.2.147.

6. Teyler, T.J., and Rudy, J.W. (2007). The hippocampal indexing theory and episodic memory: updating the index. Hippocampus *17*, 1158–1169. https://doi.org/10.1002/hipo.20350.

7. Leutgeb, S., Leutgeb, J.K., Barnes, C.A., Moser, E.I., McNaughton, B.L., and Moser, M.-B. (2005). Independent codes for spatial and episodic memory in hippocampal neuronal ensembles. Science *309*, 619–623. https://doi.org/10.1126/science.1114037.

8. Sutherland, R.J., and Lehmann, H. (2011). Alternative conceptions of memory consolidation and the role of the hippocampus at the systems level in rodents. Curr. Opin. Neurobiol. *21*, 446–451. https://doi.org/10.1016/j.conb.2011.04.007.

9. Frankland, P.W., and Bontempi, B. (2005). The organization of recent and remote memories. Nat. Rev. Neurosci. *6*, 119–130. https://doi.org/10.1038/nrn1607.

10. Marr, D. (1970). A theory for cerebral neocortex. Proc. R. Soc. Lond. B Biol. Sci. *176*, 161–234. https://doi.org/10.1098/rspb.1970.0040.

11. McClelland, J.L., McNaughton, B.L., and O'Reilly, R.C. (1995). Why there are complementary learning systems in the hippocampus and neocortex: insights from the successes and failures of connectionist models of learning and memory. Psychol. Rev. *102*, 419–457. https://doi.org/10.1037/0033-295X.102.3.419.

12. Mishkin, M., Vargha-Khadem, F., and Gadian, D.G. (1998). Amnesia and the organization of the hippocampal system. Hippocampus *8*, 212–216. https://doi.org/10.1002/(SICI)1098-1063(1998)8:3<212::AID-HIPO4>3.0.CO;2-L.

13. Moscovitch, M., Nadel, L., Winocur, G., Gilboa, A., and Rosenbaum, R.S. (2006). The cognitive neuroscience of remote episodic, semantic and spatial memory. Curr. Opin. Neurobiol. *16*, 179–190. https://doi.org/10.1016/j.conb.2006.03.013.

14. Tse, D., Langston, R.F., Kakeyama, M., Bethus, I., Spooner, P.A., Wood, E.R., Witter, M.P., and Morris, R.G.M. (2007). Schemas and memory consolidation. Science *316*, 76–82. https://doi.org/10.1126/science.1135935.

15. Wiltgen, B.J., and Silva, A.J. (2007). Memory for context becomes less specific with time. Learn. Mem. *14*, 313–317. https://doi.org/10.1101/lm.430907.

16. Esteves, I.M., Chang, H., Neumann, A.R., Sun, J., Mohajerani, M.H., and McNaughton, B.L. (2021). Spatial information encoding across multiple neocortical regions depends on an intact Hippocampus. J. Neurosci. *41*, 307–319. https://doi.org/10.1523/JNEUROSCI.1788-20.2020.

17. Mao, D., Neumann, A.R., Sun, J., Bonin, V., Mohajerani, M.H., and McNaughton, B.L. (2018). Hippocampus-dependent emergence of spatial sequence coding in retrosplenial cortex. Proc. Natl. Acad. Sci. USA *115*, 8015–8018. https://doi.org/10.1073/pnas.1803224115.

18. Minderer, M., Brown, K.D., and Harvey, C.D. (2019). The spatial structure of neural encoding in mouse posterior cortex during navigation. Neuron *102*, 232–248.e11. https://doi.org/10.1016/j.neuron.2019.01.029.

19. Saleem, A.B., Diamanti, E.M., Fournier, J., Harris, K.D., and Carandini, M. (2018). Coherent encoding of subjective spatial position in visual cortex and hippocampus. Nature *562*, 124–127. https://doi.org/10.1038/s41586-018-0516-1.

20. Mao, D., Kandler, S., McNaughton, B.L., and Bonin, V. (2017). Sparse orthogonal population representation of spatial context in the retrosplenial cortex. Nat. Commun. *8*, 243. https://doi.org/10.1038/s41467-017-00180-9.

21. Skaggs, W.E., McNaughton, B.L., and Gothard, K.M. (1992). An Information-Theoretic Approach to Deciphering the Hippocampal Code (In NIPS).

22. Ferbinteanu, J., Ray, C., and McDonald, R.J. (2003). Both dorsal and ventral hippocampus contribute to spatial learning in Long-Evans rats. Neurosci. Lett. *345*, 131–135. https://doi.org/10.1016/s0304-3940(03)00473-7.

23. Moser, M.B., Moser, E.I., Forrest, E., Andersen, P., and Morris, R.G. (1995). Spatial learning with a minislab in the dorsal hippocampus. Proc. Natl. Acad. Sci. USA *92*, 9697–9701. https://doi.org/10.1073/pnas.92.21.9697.

24. Sekeres, M.J., Neve, R.L., Frankland, P.W., and Josselyn, S.A. (2010). Dorsal hippocampal CREB is both necessary and sufficient for spatial memory. Learn. Mem. *17*, 280–283. https://doi.org/10.1101/lm.1785510.

25. Cenquizca, L.A., and Swanson, L.W. (2007). Spatial organization of direct hippocampal field CA1 axonal projections to the rest of the cerebral cortex. Brain Res. Rev. *56*, 1–26. https://doi.org/10.1016/j.brainresrev.2007.05.002.

26. Miyashita, T., and Rockland, K.S. (2007). GABAergic projections from the hippocampus to the retrosplenial cortex in the rat. Eur. J. Neurosci. *26*, 1193–1204. https://doi.org/10.1111/j.1460-9568.2007.05745.x.

27. Sugar, J., Witter, M.P., van Strien, N.M., and Cappaert, N.L.M. (2011). The retrosplenial cortex: intrinsic connectivity and connections with the (para)hippocampal region in the rat. An interactive connectome. Front. Neuroinform. *5*, 7. https://doi.org/10.3389/fninf.2011.00007.

28. Wyss, J.M., and Van Groen, T. (1992). Connections between the retrosplenial cortex and the hippocampal formation in the rat: a review. Hippocampus *2*, 1–11. https://doi.org/10.1002/hipo.450020102.

29. Pachitariu, M., Stringer, C., Dipoppa, M., Schröder, S., Rossi, L.F., Dalgleish, H., Carandini, M., and Harris, K.D. (2017). Suite2p: Beyond 10,000 Neurons with Standard Two-Photon Microscopy, p. 061507. https://doi.org/10.1101/061507.

30. Bonin, V., Histed, M.H., Yurgenson, S., and Reid, R.C. (2011). Local diversity and fine-scale organization of receptive fields in mouse visual cortex. J. Neurosci. *31*, 18506–18521. https://doi.org/10.1523/JNEUROSCI.2974-11.2011.

31. Pnevmatikakis, E.A., Soudry, D., Gao, Y., Machado, T.A., Merel, J., Pfau, D., Reardon, T., Mu, Y., Lacefield, C., Yang, W., et al. (2016). Simultaneous denoising, deconvolution, and demixing of calcium imaging data. Neuron *89*, 285–299. https://doi.org/10.1016/j.neuron.2015.11.037.

32. Chang, H., Esteves, I.M., Neumann, A.R., Sun, J., Mohajerani, M.H., and McNaughton, B.L. (2020). Coordinated activities of retrosplenial ensembles during resting-state encode spatial landmarks. Philos. Trans. R. Soc. Lond. B Biol. Sci. *375*, 20190228. https://doi.org/10.1098/rstb.2019.0228.

33. Zhang, K., Ginzburg, I., McNaughton, B.L., and Sejnowski, T.J. (1998). Interpreting neuronal population activity by reconstruction: unified framework with application to hippocampal place cells. J. Neurophysiol. *79*, 1017–1044. https://doi.org/10.1152/jn.1998.79.2.1017.

STAR★METHODS

KEY RESOURCES TABLE

REAGENT or RESOURCE	SOURCE	IDENTIFIER
Chemicals, peptides, and recombinant proteins		
N-methyl-D-aspartic acid (NMDA)	Sigma-Aldrich	Cat#M3262; CAS: 6384-92-5
Experimental models: Organisms/strains		
Thy1-GCaMP6s	The Jackson Laboratory	RRID:IMSR_JAX:024275
C57BL/6 (colony breeding pair)	Charles River Laboratories	RRID:MGI:5656552
Software and algorithms		
MATLAB R2018b	MathWorks	https://matlab.mathworks.com/
SPSS 28.0.1.0	IBM	https://www.ibm.com/support/pages/downloading-ibm-spss-statistics-28010
Suite2p	Pachitariu et al., 2017[29]	https://github.com/MouseLand/suite2p

RESOURCE AVAILABILITY

Lead contact

Further information and requests should be directed to and will be fulfilled by the lead contact, Ingrid Esteves (ingrid.esteves@uleth.ca).

Materials availability

This study did not generate new unique reagents.

Data and code availability

- All data reported in this paper will be shared by the lead contact upon request.
- This paper does not report original code.
- Any additional information required to reanalyze the data reported in this paper is available from the lead contact upon request.

EXPERIMENTAL MODEL AND SUBJECT DETAILS

Fifteen adult transgenic Thy1-GCaMP6s mice (20–25 g; 2 months old at the time of surgery; 9 males and 6 females) were used in this study. Animals were randomly divided into two groups: Lesion (n = 10; bilateral hippocampal lesion), Sham (n = 5; sham lesion). Four animals of the Lesion group were excluded from data analysis for not exhibiting a considerable amount of hippocampal lesion. Additionally, the histology of all animals included in this study did not exhibit any lesions outside the hippocampus region (see Figure S1). Experiments were conducted between 7:30 a.m. and 7:30 p.m. Following surgery, animals were single-housed in standard rodent cages, maintained at 24°C room temperature and under a 12h light/dark cycle (lights on at 7:30 a.m.), with free access to food and water before the beginning of training.

Ethics

All animal procedures were conducted in compliance with the guidelines established by the Canadian Council for Animal Care, and were approved by the Animal Welfare Committee of the University of Lethbridge.

METHOD DETAILS

Experimental design

We used two-photon Ca2+ imaging to record Thy1-GCaMP6s mice during virtual navigation before and after bilateral lesions of the dorsal hippocampi. A 5 mm cranial window was implanted above the dorsal cortex, and we tracked neuronal activity of three different neocortical areas: retrosplenial cortex (RSC),

secondary motor cortex (M2), and the primary hindlimb somatosensory cortex (S1) (Figure 1A). Water restricted motivated mice were trained over a period of ~1 month to run and head-fixed over a 150 cm long treadmill belt, where they receive a drop of sucrose water at the end of each lap (Figure 1B). After training, mice were exposed to the 'familiar' belt for 10 consecutive days (belt 1; Figure 1C), while imaging was carried out on layers II/III of RSC. Animals then started to run for 10 consecutive days alternatingly during the same session on this familiar and on a pre-lesion novel belt, with different tactile cues placed on distinct locations (belt 2; Figure 1C), while still recording from the RSC. On the last five days of the pre-operatively (sham/lesion) phase, we tracked spatial activity across layers II/III of areas M2 and S1, also alternating using the familiar belt along with the pre-operatively novel belt. During the post-operatively phase, bilateral excitotoxic lesion (or sham) of the dorsal hippocampi was then carried out using N-methyl-D-asparate (NMDA). After a one month of recovery, RSC neuronal activity was again recorded while animals ran for 8 days on the familiar belt. Subsequently, mice ran for 10 more days, alternating on the pre-operatively familiar belt and on a post-operatively novel belt, which the animals never experienced before lesion/sham surgery (belt 3; Figure 1C). At the end, imaging was also carried out on M2 and S1 regions using both Familiar (belt 1) and Novel belt (belt 3; Figure 1D).

All the animals included in the lesion group exhibited tissue loss in the dorsal hippocampal formation, with remaining volume of at least 50%, compared to the sham group (Figure 1E). All animal procedures were conducted in accordance with the guidelines established by the Canadian Council on Animal Care, using protocols approved by the Animal Welfare Committee of the University of Lethbridge.

Head plate and imaging window implantation

All surgical procedure (head plate fixation, cranial window, and hippocampal window) was performed under aseptic conditions as described in.[16] Briefly, prior to surgery animals were injected with buprenorphine (0.1 mg/kg, subcutaneous), dexamethasone (2 mg/kg, intramuscular), and 0.5 mL of dextrose 5% (D5W) with atropine (0.06 mg/kg, subcutaneous). Then, mice were anesthetized with isoflurane (1%–1.5%, O2: 1 L/min), and placed in a stereotaxic frame. Lidocaine (0.5%, 7 mg/kg) was injected subcutaneously under the incision site before the skull was exposed and a custom-made titanium head-plate was fixed using adhesive cement (C&B-metabond, Parkell). A 5 mm diameter craniotomy was made following bregma-referenced coordinates: 1.5 mm anterior to −3.5 mm posterior; ±2.5 mm medial-lateral (Figure 1A). A window, composed of a 7 mm diameter round coverslip stacked over two 5 mm diameter coverslips (affixed with optical adhesive NOA71, Norland), were implanted over the craniotomy. Finally, a rubber ring was fixed over the head-plate to form a well to retain water between the imaging region and the immersion objective during recording (Figure 1B). During the entire procedure, animals' temperature was maintained at 37°C using a heating pad. Post-operative analgesic treatment was continued with meloxicam (Metacam, 10 mg/kg, subcutaneous) and enrofloxacin (Baytril, 10 mg/kg, subcutaneous) for 3 days after surgery.

Treadmill training and two-photon imaging

Mice were allowed to recover for one week following the implantation of the cranial window. Subsequently, water restriction started and training sessions was then carried out over a period of one month.

Three days before the water restriction began, we weighed each animal at the same time each day to establish the baseline weight. The baseline weight was calculated as the average of the three daily weights. Water and food were given concurrently during 30 min to the animals in their home cages 6–8 h after training/imaging sessions. Animal weights were recorded daily around the same time in a water restriction log sheet for the entire duration of the water restriction period. Water restriction was discontinued while animals were recovering from lesion/sham surgery (approximately 1 month).

During the training sessions, mice were head fixed and progressively trained to run for reward over a 150 cm long linear treadmill belt lined with tactile cues. The duration of each session gradually increased form 10 min to 1 h, and imaging session started once performance reached over 50 laps per hour. Both the imaging and training treadmill consisted of a 150 cm Velcro (Country Brook) belt mounted with tactile cues (made of hot-glue stripes, reflective tape, and Velcro) inserted at several locations (Figure 1C). The belt was looped around two polyamide wheels (10 cm in diameter), separated by 40 cm, and attached to both ends of the treadmill. An optical encoder (Avago Tech) attached to the front wheel shaft was used to decode the animal position. A photoelectric sensor (Omron) and a reflective tape attached to the

opposite side of the belt was used to trigger the reward (~2.5 μL of sucrose water 10%) at the same location of the belt for all trials. A solenoid pinch valve (Bio-Chem) was used to dispense the reward in a metal spout in front of the animal's mouth upon completion of one lap, and licking activity was monitored with a capacitive sensor attached to the spout. The reward delivery, the encoder and the licking sensor was controlled using a custom-designed circuit with a microcontroller (Arduino UNO, Farnell).

Two-photon calcium imaging sessions was conducted using a Thorlabs Bergamo II multi-photon microscope with a galvo/resonant X-Y mirrors scanning at a frame rate of 19 Hz. A GCaMP6s was excited with a Ti:Sapphire pulsed laser (Coherent) with a fixed wavelength of 920 nm (~80 mW output power measured at the sample). The microscope was equipped with a GaAsP photomultiplier tube (Hamamatsu) to detect and amplify the fluorescent lights emitted. Images were acquired through a 16× water-immersion objective (Nikon, 0.8 N.A.). Field of view (FOV) was 835 × 835 μm in size, at a resolution of 800 × 800 pixels, and at depths between 130 μm and 190 μm (layers II/III). Imaging frames and treadmill signals were synchronized using Clampex software (Axon Instruments). Imaging was performed in three different neocortical areas (RSC, M2, and S1) and FOV was placed so that as many excitatory neurons as possible were depicted (left or right hemisphere).

Hippocampal lesion

After the imaging session of the pre-operative phase was concluded, animal were anesthetized again for the bilateral hippocampal lesions. Phenobarbital (30–40 mg/kg, intraperitoneal) was administered 1 h prior to anesthesia as an anticonvulsant. Animals were then anesthetized using isoflurane (1%–1.5%, O2: 1 L/min), and placed again in a stereotaxic frame. Using a high-speed dental drill with sterile bit, the coverslips was removed, the brain was exposed, and NMDA (15 mg/mL, NMDA in 1× PBS) was injected at four injection sites (2 in each hemisphere): −2.3 mm AP, 1.5 mm ML, 1.8 mm DV and, −3.2 mm AP, 2.5 mm ML, 2.0 mm DV. A micropipette, with tip diameter between 20 μm and 30 μm, secured onto a Nanoject II (Drummond Sci.) injection device was used during the NMDA infusions. Each injection site received 73.6 nL of the NMDA solution over a 2 min period (9.2 nL/pulse × 8pulses; inter-pulse interval: 15s). After each injection, the NMDA was allowed to disperse over a 5 min period and the micropipette was slowly withdrawn. Sham animals received only the micropipette trauma (penetration but no injection of NMDA-filled micropipette on the four injection sites). Once the injections were completed, a new coverslip was re-implanted and the animal was allowed to recover. NMDA vehicle was not used in the sham animals because we were avoiding any unnecessary tissue damage or potential loss of function that could be caused by controlling for the injected volume. Considering that our goal was to evaluate the impact of the dorsal hippocampal lesion, rather than isolating the pharmaceutical effect of NMDA, we lowered the pipette tips for the sham group to control for unwanted consequences, such as puncturing the lateral ventricles. Diazepam (5 mg/kg, intraperitoneal) was administered right after surgery to suppress potential seizures. Meloxicam (Metacam, 10 mg/kg, subcutaneous) and enrofloxacin (Baytril, 10 mg/kg, subcutaneous) were also administered for 3 days after surgery. Members of the sham group received the same injections of diazepam, meloxicam and enrofloxacin in order to properly control for the injected drugs. The post-operatively phase started after a 1-month period following the lesion, to allow for the excitotoxic lesion to stabilize.

Image pre-processing

To extract the calcium fluorescence signal, the acquired image time series for each session was pre-processed using the Suite-2p software.[29] This toolbox automatically perform motion correction for each frame, detects the regions of interest (ROI) as candidate cells, and extracts the fluorescence signal for each ROI. The candidate neurons detected by Suite-2p were visually inspected and labeled as a cell based on their morphology (with spatial mask overlying cell bodies) and fluorescence trace (with distinct calcium deflections). We subtracted the neuropil contamination from the neuronal fluorescence signal used for analysis, and the ratio ΔF/F time-courses was obtained for each cell.[30] Briefly, this is achieved by dilating the ROI mask of individual neurons by 8 pixels, corresponding roughly to 8 microns, and subtracting this dilated mask from the original mask to obtain an outer ring. Raw neuropil fluorescence was computed from the mean intensities of these outer ring masks. The neuropil signal is subsequently extracted by reconstructing the fluorescent time-series of the neuropil associated with each neuron using the first component obtained from singular value decomposition over all the raw neuropil time-series. The spiking rates for each neuron was inferred by deconvolving the ΔF/F time-courses using the algorithm provided by Pnevmatikakis et al., 2016.[31] Briefly, this is achieved by fitting the fluorescence time-series to a second-order autoregressive

function, where a given input of spikes causes the fluorescence levels to deviate from baseline with fixed rise and decay constants, as reflective of the dynamics in intracellular calcium concentration and of the fluorophore. The estimation of the instantaneous input of spikes that gives rise to individual transients, given the estimates of the rise and decay constants, yields the final deconvolved time-series. All data analyses were conducted on the deconvolved time-courses using MATLAB (R2018b Mathworks, Natick, MA).

Place field analysis

To be classified as spatially selective, neurons had to pass the following criteria:

We first obtained the spatial information (SI) of each neuron and a shuffled distribution of SI by circularly shifting the time courses 1000 times, as described in.[16] Neurons with SI higher than the 95th percentile of the shuffled distribution were selected as potential spatially selective cell. Next, we computed the spatial tuning characteristics of place fields by obtaining a continuous wavelet transform over the spatial response curve of each neurons that passed the SI criteria, as described in.[32] The local maxima in the transform indicate the location and the width of place fields. A threshold of 3 median absolute deviations from the median of the wavelet coefficients at the lowest scale was used. Cells with peaks values lower than the threshold, and cells with peaks that fell within the receptive field of a local maximum at a higher scale were rejected. Besides the first two criteria mentioned above, to be classified as spatially selective cells the mean activity within a place field was required to be 2.5 times higher than the mean activity outside of place field, peak activity was required to occur inside the place field in at least a third of the laps, and field width must be wider than 7.5 cm or narrower than 120 cm.

Bayesian decoder

A naive Bayesian classifier was implemented to decode animals' locations with respect to the population activities.[16,17,32,33] The maximum log-posterior probability was obtained as the decoded location:

$$\max_x l\left(\frac{x}{n}\right) \propto \sum_{i=1}^{N} n_i \log(f_i(x)) - \delta t \sum_{i=1}^{N} f_i(x) + \log(P(x))$$

Here, n_i is the activity of neuron i in a sample of N simultaneously imaged neurons for a given recording frame. $f_i(x)$ is the mean activity of neuron i at position x (expressed in units of $\Delta F F^{-1} s^{-1}$) smoothed using a Gaussian kernel of $\sigma = 4$ cm. n_i were derived within time bins of width $\delta t = 1$ s (by moving sum where the activities per frame were normalized to $\Delta F F^{-1} s^{-1}$). Finally, $P(x)$ is the probability of occupancy at distinct spatial bins x, of which there are 150. Firing rates of zero in $f_i(x)$ (which normally leads to the undesirable condition of $\log 0 = -inf$) were replaced by a constant penalty term of 2^{-52} ('eps' under MATLAB).

Decoding error was assessed by leave-one-out cross-validation, where for k trials $k - 1$ trials are used to derive $f_i(x)$ and $P(x)$, and n_i is obtained from the left-out trial from which locations are decoded. This process is repeated for each trial within a given recording session. Error is calculated as the absolute distance between actual and decoded locations. Due to the belt being circular, errors were measured as circular distances (i.e., the shortest distance between the actual and decoded positions).

Histology

At the end of all imaging sessions, animals were deeply anesthetized with sodium pentobarbital (Euthanyl, 100 mg/kg), and perfused transcardially with PBS followed by 4% paraformaldehyde. Brains remained in 4% paraformaldehyde for 2 days and then cryoprotected in 30% sucrose solution before sectioning. Coronal sections were cut using a sliding microtome at a thickness of 40 μm. Images from the section were obtained using a NanoZoomer scanning microscope (Hamamatsu Photonics), and the extent of the dorsal hippocampal lesion were evaluated for each animal using the coronal sections from −1 to −3.5 mm AP. The volume of remaining hippocampal tissue of each animal from the lesion and sham group are shown in Figure 1E.

QUANTIFICATION AND STATISTICAL ANALYSIS

All statistical tests performed in this work were conducted using IBM SPSS Statistics for Windows, version 28.0.1.0 (IBM Corp., Armonk, N.Y., USA). Further details of all statistical tests implemented in this study are provided in each figure.